AIAA JOURNAL
Vol. 48, No. 9, September 2010

Variable-Kinematics Approach for Linearized Buckling Analysis of Laminated Plates and Shells

M. D'Ottavio*
Université Paris Ouest, 92410 Ville d'Avray, France
and
E. Carrera
Politecnico di Torino, 10129 Torino, Italy

DOI: 10.2514/1.J050203

This work deals with the linearized buckling analysis of laminated plates and shells. A variable-kinematics approach with hierarchical capabilities is considered to establish the accuracy of a large variety of classical and advanced plate/shell theories in order to evaluate buckling loads. So-called equivalent-single-layer as well as layerwise-variable descriptions are implemented. Interlaminar continuity of transverse shear and normal stresses are a priori fulfilled by referring to Reissner's mixed variational theorem. Stability equations are derived in compact form by referring to Carrera's unified formulation for the most general case of doubly curved shells. The eigenvalue problem is solved in the case of closed-form solutions related to simply supported boundary conditions and axially loaded multilayered plates/shells made of orthotropic layers. The cases of axial constant strains and constant stresses are considered and compared to available three-dimensional and two-dimensional results. Results related to Love and Donnell approximations are implemented for comparison purposes. The accuracy of various approximations is established for significant multilayered plate and shell problems.

Nomenclature

A	=	membrane stiffness of the laminate
a, b	=	in-plane plate/shell dimensions
$\tilde{C}$	=	stiffness coefficient in the global reference frame
C^*	=	plane stress reduced stiffness coefficient
D^*	=	plane stress bending stiffness of the laminate
E_L	=	Young's modulus in the fiber direction
E_T	=	Young's modulus in the transverse direction
$F_\tau(z)$, $F_s(z)$	=	thickness expansion polynomials (τ, $s \in [1, N]$)
G	=	shear modulus
H	=	shell metric coefficient
h	=	thickness of the plate/shell
$\mathbf{K}$	=	linear stiffness matrix
$\mathbf{K}_\sigma$	=	geometric stiffness matrix
k	=	layer index
m, n	=	number of half-waves along α, β
N	=	order of polynomial expansion
N_l	=	number of layers
N^ϵ_{cr}	=	critical load per unit length for a uniform initial strain
N^σ_{cr}	=	critical load per unit length for a uniform initial stress
n'	=	circumferential full wave number
R	=	curvature radius
S	=	aspect ratio a/h
u_i	=	displacement vector
z	=	rectilinear thickness coordinate
α, β	=	curvilinear in-plane coordinates
ϵ_{ij}	=	strain tensor
ϵ^0	=	uniform initial strain
κ	=	shear correction factor
λ	=	scalar load factor
ν	=	Poisson's ratio
σ_{ij}	=	stress tensor
σ^0	=	uniform initial stress
χ	=	biaxial load ratio
Ω	=	shell surface

I. Introduction

BUCKLING is one of the characteristic failure modes of slender structures such as plates and shells. It consists of a sudden change in the shell geometry at a critical load, which can be rather harmless, as in flat plates, or induce a drastic reduction in the load-carrying capability, as in cylindrical shells. This latter behavior is additionally affected to a great extent by small perturbations (imperfections) of the nominal initial configuration, which can lead to catastrophic failures at load levels far below those predicted by a simplified analysis method. Because of this unstable behavior, the most general approach for buckling failure analyses requires complex nonlinear equilibrium and stability equations to be solved [1,2]. Moreover, these computationally expensive solutions should be used together with a reliability analysis to cope with the probabilistic nature of real perturbation sources [3].

A simplified method for buckling analysis can be devised by interpreting the critical load as the load at which more than one infinitesimally adjacent equilibrium configuration exists (bifurcation point). If a linear initial equilibrium path is also assumed, the linearized stability analysis reduces the determination of the critical load to a linear eigenvalue problem (Euler's method) [4]. This simplified approach can conveniently be applied to flat plates, since the critical equilibrium configuration shows a gradual geometry change when the load passes through the critical level.

An extension of the eigenvalue approach to imperfection-sensitive cylindrical shells has been proposed by retaining a nonlinear prebuckling deformation [5]. However, despite today's computing performances, which offer a robust nonlinear stability analysis, the conservative lower-bound design philosophy developed in shell design practice in the late 1960s and 1970s is still widely used [6,7]. In this design method, the allowable critical load predicted through linearized analysis is reduced by an empirical knockdown factor that accounts for the degrading effects of the uncertainties and

Received 10 September 2009; revision received 26 May 2010; accepted for publication 2 June 2010.

*Laboratoire Energétique Mécanique Electromagnétisme, Department of Aerospace Engineering, 50 rue de Sèvres; michele.d_ottavio@u-paris10.fr (Corresponding Author).

imperfections associated with the geometry, material, loading, and boundary conditions. Efforts are currently directed toward an improvement of the excessively conservative and deterministic knockdown factors originally found for isotropic shells upon consideration of composite fabrication processes and probabilistic aspects [8–10]. On the basis of the above considerations, this paper will employ the classical Euler method to predict bifurcation loads of both composite plates and cylindrical shells. The authors are aware that in the case of cylindrical shells, the computed buckling loads require the use of adequate knockdown factors.

Finally, it is emphasized that linearized stability analysis makes sense if, and only if, the buckled configuration is on an equilibrium path that is different from that of the initial loading (bifurcation buckling). A sufficient condition for the existence of bifurcation buckling is that the initial in-plane loading does not produce an out-of-plane (transverse) deformation [11,12]. Furthermore, the calculation of the buckling load as a bifurcation point fails when the shell exhibits snap-through phenomena [2]. If at least one of these conditions is violated, a nonlinear analysis would be necessary, a topic that is out of the scope of the present contribution. Therefore, this work shall be limited to symmetric laminates and axially loaded cylindrical shells.

Since significant geometric nonlinearities arise from changes in the membrane stiffness, buckling loads are usually classified as a global structural parameter. Hence, due to the inherent slenderness of buckling structures and in order to limit the computational effort, simple two-dimensional (2-D) plate/shell models that rely on Kirchhoff–Love or Mindlin–Reissner kinematics appear to be sufficiently accurate for the prediction of critical loads (see, for example, [13]). However, it is well known that a rational design of composite structures requires dedicated models in order to cope with their complex behavior due to the heterogeneous multilayered cross section, the characteristic transverse shear deformability, and the coupled membrane bending–twisting response [14–17]. These peculiarities increase the complexity of the buckling behavior of composite shells [18–22]. For example, different global and local instabilities occur in compressed sandwich structures, which depend not only on the geometric ratios, but also on the ratio between the stiffness of the faces and that of the core [23].

Different shell formulations (in particular, those associated with the Donnell, Love, and Koiter-Sanders hypotheses) have been assessed with respect to anisotropic behavior of composite laminates (see, for example, [24,25]). However, to the best of the authors' knowledge, a rigorous assessment of the 2-D approximations against buckling of composite plate/shell models is still missing. The question concerning the quality of the description of transverse behavior in composite panels is pertinent, especially when the effects of boundary layers and/or damageable material behavior (in particular, delamination) has to be accounted for.

In recent years, a hierarchic approach with variable-kinematics 2-D models for composite plates and shells has successfully been developed by Carrera (see, for example, the original contribution in [26], the summary provided in [27], the finite element implementation in [28,29], and the recent application in [30]). By referring to two different variational formulations as well as to equivalent-single-layer and layerwise descriptions, hierarchically ordered approximations are introduced for the through-thickness behavior by means of a compact unified notation. Carrera's unified formulation (CUF) thus permits a systematic assessment of a large number of plate/shell models, whose accuracy has been demonstrated to range from classical 2-D models to quasi-3-D descriptions for both free-vibration problems and static stress analysis (see, for example, [31,32]). In this paper, CUF has been developed and applied to perform buckling analyses of laminated plates and shells. The variable-kinematics modeling technique based on CUF is briefly recalled in Sec. II, in which several possible definitions of the geometric stiffness matrix are dealt with in detail. An assessment of the proposed models of simply supported laminated plates and shells is proposed in Sec. III in terms of a closed-form solution based on Navier's method. Preliminary results concerning the bending of plates are recalled in Sec. III.A referring to the classical Pagano problem. This approach is subsequently applied to the linearized buckling analysis of laminated plates (Sec. III.B) and of open as well as closed cylindrical shells (Sec. III.C). The role of characteristic design parameters, such as aspect ratio and curvature radius, is highlighted. All the results are presented in tables to facilitate a detailed comparison with other models proposed in literature. Finally, the main findings are summarized in Sec. IV.

II. Variable-Kinematics Modeling

The variable-kinematics modeling technique based on CUF has already been presented with due detail in numerous papers (see, for example, [31,32] for plate and [33–35] for shell applications). Therefore, in the following, only a brief description of CUF will be given and the principal features of the resulting models will be summarized.

A. Hierarchic Models in Carrera's Unified Formulation

Reduced plate/shell models may be classified as classical and advanced with reference to the satisfaction of the so-called C_z^0 requirements: i.e., the satisfaction of transverse equilibrium at the layers' interfaces and the representation of the slope discontinuity of the displacement field along the composite cross section [36]. Classical models are based on the principle of virtual displacements (PVD) and the introduction of approximations for the three displacement components $u_i = [\,u_x \quad u_y \quad u_z\,]^T$. The stress field is obtained from the compatible strains by means of the constitutive equation, and therefore equilibrium at the interfaces may be not satisfied. Advanced models refer to Reissner's partially mixed variational theorem (RMVT), which permits introducing independent approximations for the displacements u_i and the transverse stress components $\sigma_{i3} = [\,\sigma_{xz} \quad \sigma_{yz} \quad \sigma_{zz}\,]^T$ [37]. Advanced models can therefore fulfill a priori the interlaminar continuity of the transverse stress field and no shear correction factors are required [38].

The assumptions for displacement unknowns can be formulated within either an equivalent-single-layer (ESL) or a layerwise (LW) description. In an ESL case, the through-thickness distribution of the displacement field is defined by variables that are defined for the whole multilayered cross section. In an LW model, assumptions are introduced for each layer separately. The relations for the multilayer are constructed with an assembly procedure that enforces the interlaminar continuity conditions. The assumptions for the transverse stress field of advanced models are always introduced within an LW description to cope with the layer-specific constitutive law. Murakami's zigzag function (MZZF) can be used to introduce within an ESL model the slope discontinuity of the displacement field at the interfaces between dissimilar materials [39]. The role of MZZF models has been thoroughly discussed in conjunction with Navier's solution and the finite element method in [40,41], respectively.

All through-thickness assumptions are formulated in terms of polynomials of order N of the thickness coordinate $x_3 = z$. ESL descriptions employ Taylor polynomials whereas LW descriptions are constructed from Legendre polynomials. In Carrera's unified formulation, linear ($N = 1$) up to fourth-order ($N = 4$) polynomials are used for all independent variables (i.e., u_i for classical PVD models and u_i and σ_{i3} for advanced RMVT models). All CUF models retain the transverse normal deformation and employ the full 3-D constitutive law. First-order shear deformation theory (FSDT) is obtained from the linear PVD-based model by penalizing the transverse normal deformation term and by introducing a shear correction factor (the standard value of $\kappa^2 = 5/6$ will be used). Classical laminated-plate theory (CLPT) is obtained by penalizing the transverse shear strain contributions of FSDT to reproduce the Kirchhoff–Love hypotheses. FSDT and CLPT models employ the reduced constitutive law referring to the plane stress condition $\sigma_{33} = 0$.

As a result, a large number of 2-D models can be constructed by selecting 1) the underlying variational formulation, 2) the multilayer description for the displacement field (ESL, ESL+MZZF, or LW), and 3) the polynomial order employed for the assumption. Each model is identified by a unique acronym that is constructed as

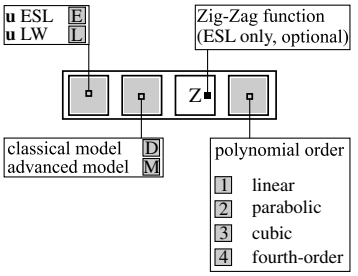

$N = 1-4$	ZZ	IC
EDN	–	–
EDZN	✓	–
LDN	✓	–
EMN	–	✓
EMZN	✓	✓
LMN	✓	✓

Fig. 1 Hierarchic unified formulation models: construction of the acronyms (left) and capability of the models to fulfill a priori the ZZ behavior and the IC (right).

illustrated in the left part of Fig. 1. The table on the right-hand side of Fig. 1 summarizes the capability of the models to a priori fulfill the C_z^0 requirements: that is, the interlaminar continuity of the transverse stress field (IC) and the slope discontinuity of the displacement field at the interfaces [zigzag (ZZ) behavior].

B. Geometry Description and Problem Definition

We consider a multilayered shell composed of N_l homogeneous, anisotropic, and perfectly bonded layers (Fig. 2). Each layer k is identified by its reference surface Ω_k and its location z_{0_k} along the panel's thickness coordinate (see Fig. 3). The in-plane curvilinear coordinates α_k and β_k are assumed to coincide with lines of principal curvature to define an orthogonal reference system on Ω_k. We will restrict the analysis to laminated shells whose principal curvature radii R_{α_k} and R_{β_k} are constant. This yields the following definition for the layer-specific metric:

$$(\mathrm{d}s_k)^2 = H_{\alpha_k}^2(\mathrm{d}\alpha_k)^2 + H_{\beta_k}^2(\mathrm{d}\beta_k)^2 + H_{\zeta_k}^2(\mathrm{d}z_k)^2 \tag{1}$$

with

$$H_{\alpha_k} = (1 + z_k/R_{\alpha_k}); \qquad H_{\beta_k} = (1 + z_k/R_{\beta_k}); \qquad H_{\zeta_k} = 1 \tag{2}$$

The class of problems considered in this work consists of simply supported biaxially loaded plates and axially loaded open cylindrical panels and closed cylindrical shells. We limit the analysis to specially orthotropic laminates, for which the bending–stretching, bending–twisting, and stretching–shearing couplings vanish. Therefore, the geometric nonlinearities will be introduced only for the direct in-plane strains $\epsilon_{\alpha\alpha}$ and $\epsilon_{\beta\beta}$; i.e., the nonlinearity of the in-plane shear deformation $\epsilon_{\alpha\beta}$ will not be included. For this class of problems we can refer to the solution method of Navier (as reported in, e.g., [42]), which gives the following expression for the displacement field $\mathbf{u} = u_i = [\,u_\alpha \quad u_\beta \quad u_3\,]$:

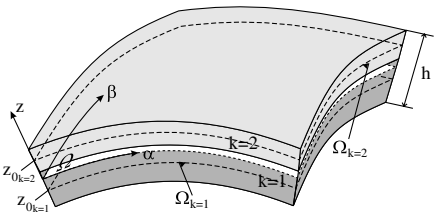

Fig. 2 Geometry description and employed notation for a multilayered shell.

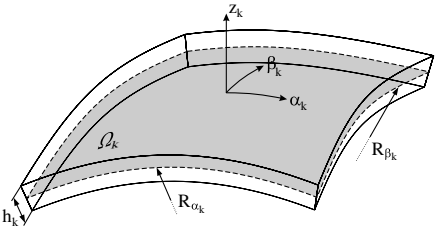

Fig. 3 Geometric parameters and coordinate system of the kth layer.

$$\begin{aligned} u_\alpha(\alpha,\beta,z) &= U_\alpha(z)\cos(\alpha/l_1)\sin(\beta/l_2);\\ u_\beta(\alpha,\beta,z) &= U_\beta(z)\sin(\alpha/l_1)\cos(\beta/l_2);\\ u_3(\alpha,\beta,z) &= U_3(z)\sin(\alpha/l_1)\sin(\beta/l_2) \end{aligned} \tag{3}$$

with $l_1 = a/(m\pi)$ and $l_2 = b/(n\pi)$, where a and b are the dimensions of the panel along α and β, respectively. The integers m and n represent the number of half-waves along the in-plane coordinates α and β, respectively.

Since the fundamental equations for linear shell problems have been reported in previous works (e.g., in [34,35]), in the following we will focus the attention only on the nonlinear terms and the construction of the geometric stiffness matrix.

C. Governing Equations for the Linearized Stability Analysis

The buckling equations are obtained according to Euler's method of adjacent equilibrium states [43]. It consists of a linearized stability analysis of an undeformed equilibrium configuration, whose critical condition is defined by a proportionally scaled load in combination with a geometric or initial stress stiffness built up from the geometric nonlinearities. The following assumptions are thus necessarily introduced:

1) The prebuckling deformation can be neglected.

2) The initial stress σ^0 remains constant and varies neither in magnitude nor in direction during buckling.

3) At bifurcation, the equilibrium states are infinitesimally adjacent so that a linearization is possible.

The buckling load can then be defined via a scalar load factor λ as the load $\sigma = \lambda\sigma^0$ for which an equilibrium configuration $\mathbf{u} \neq \mathbf{0}$ exists such that

$$\delta\mathbf{u}^T[\mathbf{K} + \lambda\mathbf{K}_\sigma(\sigma^0)]\mathbf{u} = \mathbf{0} \tag{4}$$

The symbol δ denotes the virtual variation and $\mathbf{K}$ is the usual linear stiffness matrix reported elsewhere. The matrix $\mathbf{K}_\sigma(\sigma^0)$ is the geometric stiffness matrix that is obtained from the expression of the work done by the virtual nonlinear strains with the actual initial stresses $\sigma^0 = [\,\sigma^0_{\alpha_k\alpha_k} \quad \sigma^0_{\beta_k\beta_k}\,]$:

$$\int_\Omega \left\{ \int_{h_k} \delta\epsilon^{nl}_{\alpha_k\alpha_k}\sigma^{0k}_{\alpha_k\alpha_k} + \delta\epsilon^{nl}_{\beta_k\beta_k}\sigma^{0k}_{\beta_k\beta_k}\,\mathrm{d}z \right\} H_{\alpha_k}H_{\beta_k}\,\mathrm{d}\alpha_k\,\mathrm{d}\beta_k \tag{5}$$

As mentioned earlier, the initial stress field does not consider transverse stresses (generalized plane stress state) or in-plane shear stresses.

1. Geometric Nonlinearities and Initial Stress Fields

The nonlinear direct in-plane strains $\epsilon_{\mu\mu}$ ($\mu = \{\alpha_k, \beta_k\}$) are expressed as [43,44]

$$\begin{aligned} \epsilon_{\mu\mu} = {} & \frac{u_{\mu,\mu}}{H_\mu} + \frac{u_3}{H_\mu R_\mu} + \frac{1}{2H_\mu^2}[(u_{\alpha_k,\mu})^2 + (u_{\beta_k,\mu})^2 + (u_{3,\mu})^2]\\ & + \frac{1}{H_\mu^2 R_\mu}(u_{\mu,\mu}u_3 - u_{3,\mu}u_\mu) + \frac{1}{2H_\mu^2 R_\mu^2}(u_3^2 + u_\mu^2) \end{aligned} \tag{6}$$

The first two terms correspond to the linear contributions ϵ^l and the last three terms to the nonlinear part ϵ^{nl}. Note that three-dimensional formulations employ the above full nonlinearities [45,46]. Simplified assumptions concerning the curvature terms may be introduced by referring to Love and Donnell's approximations for thin and shallow shells, respectively. These are introduced in the linear strain components as reported in, for example, [34,35]. Donnell's approximation amounts to retain only the first three terms of Eq. (6). Within Love's thin-shell approximation, we neglect z/R_μ with respect to unity; i.e., we set $H_\mu = 1$ in Eq. (6).

Two-dimensional shell models often refer to von Kàrmàn's approximation, which retains only the nonlinear contribution of the deflection u_3 [42]:

$$\epsilon_{\mu\mu} = \frac{u_{\mu,\mu}}{H_\mu} + \frac{u_3}{H_\mu R_\mu} + \frac{(u_{3,\mu})^2}{2H_\mu^2} \tag{7}$$

In this case, Donnell's approximation does not affect the nonlinear part of the direct in-plane strains.

Two different definitions of the initial stress $\sigma^{0k}_{\mu\mu}$ will be considered, which leads to two alternate formulations for the geometric stiffness matrix. In one case, we define a uniform stress that is constant over the thickness of the laminate (i.e., $\sigma^{0k}_{\mu\mu} = \sigma^0_{\mu\mu}$ for all layers of the laminate). In the other case, we use a uniform strain $\epsilon^0_{\mu\mu}$ that produces a layerwise uniform stress state $\sigma^{0k}_{\mu\mu}$. In the latter case, the initial stress in each layer will be proportional to the elasticity coefficient of the layer and will be defined according to [45,47] as

$$\sigma^{0k}_{\alpha\alpha} = \tilde{C}^k_{11}\epsilon^0_{\alpha\alpha}; \qquad \sigma^{0k}_{\beta\beta} = \tilde{C}^k_{22}\epsilon^0_{\beta\beta} \tag{8}$$

A biaxial prestress state is introduced in terms of a constant ratio χ that is defined as $\chi = \epsilon^0_{\beta\beta}/\epsilon^0_{\alpha\alpha}$ for the uniform strain formulation and as $\chi = \sigma^0_{\beta\beta}/\sigma^0_{\alpha\alpha}$ for the uniform stress formulation.

2. *Two-Dimensional Approximations in CUF*

The plate/shell model is constructed upon introducing the thickness assumptions in Carrera's unified formulation for the displacement field $\mathbf{u}$:

$$\delta\mathbf{u}(\alpha,\beta,z) = F_\tau(z)\delta\hat{\mathbf{U}}_\tau(\alpha,\beta) \quad \text{and} \quad \mathbf{u}(\alpha,\beta,z) = F_s(z)\hat{\mathbf{U}}_s(\alpha,\beta) \tag{9}$$

where $k = 1, 2, \ldots, N_l$ is the layer index and τ, $s = 1, 2, \ldots, N$ are the indexes for the polynomial approximations. Subsequently, the derivatives of the trigonometric functions in Eq. (3) are carried out explicitly and the mode numbers (m, n) appear in the stiffness matrices. The governing equation (4) can be rewritten within CUF in terms of the 3×3 *fundamental nuclei* for the kth layer and for each pair (τ, s) as follows:

$$\delta\mathbf{U}^k_{\tau(mn)}: [\mathbf{K}^{k\tau s}_{(mn)} + \lambda\mathbf{K}^{k\tau s}_{\sigma(mn)}]\mathbf{U}^k_{s(mn)} = \mathbf{0} \tag{10}$$

The fundamental nucleus of the linear stiffness matrix $\mathbf{K}^{k\tau s}_{(mn)}$ can be found elsewhere [34,35]; that for the geometric stiffness matrix $\mathbf{K}^{k\tau s}_{\sigma(mn)}$ is reported in the Appendix. The construction of the system of equations for the whole multilayer shell follows the standard assembly procedure reported in the already mentioned literature on CUF.

Among all possible buckling modes defined by a pair (m, n), the lowest eigenvalue $\lambda_{(mn)}$ indicates the *critical* buckling load for the whole laminate of thickness h according to

$$N_{\text{cr}} = \lambda_{(mn)}\sigma^0_{\alpha_k\alpha_k}h \tag{11}$$

for the initial stress formulation and to

$$N_{\text{cr}} = \sum_{k=1}^{N_l}\int_{h_k}\tilde{C}^k_{11}\,\text{d}z(\lambda_{(mn)}\epsilon^0_{\alpha_k\alpha_k}) = \tilde{A}_{11}\lambda_{(mn)}\epsilon^0_{\alpha_k\alpha_k} \tag{12}$$

for the initial strain formulation. Note that for simplicity, a unitary preload can be considered: i.e., $\epsilon^0_{\alpha_k\alpha_k} = 1$ or $\sigma^0_{\alpha_k\alpha_k} = 1$.

III. Numerical Results and Discussion

According to the findings in [11,12], the calculation of buckling loads as a bifurcation point will be limited to symmetric laminates. Furthermore, the analysis of curved shells will be restricted to axially loaded open cylindrical panels and closed hollow cylinders. Three different specially orthotropic composite materials will be considered for the numerical examples employed to assess the proposed hierarchic models:

Material 1 is a symmetric three-layered carbon-fiber-reinforced polymer (CFRP) laminate with layup [0/90/0] and the following elastic properties for the ply: $E_L/E_T = 25$, $G_{LT}/E_T = 0.5$, $G_{TT}/E_T = 0.2$, and $\nu_{LT} = \nu_{TT} = 0.25$ [48].

Material 2 is a symmetric CRFP laminate [0/90/...] with an odd number of layers N_l. The total thickness of the 0 and 90° layers is the same and the outer layers are at 0°. Each ply has the following elastic properties: E_L/E_T variable, $G_{LT}/E_T = 0.6$, $G_{TT}/E_T = 0.5$, and $\nu_{LT} = \nu_{TT} = 0.25$ [47].

Material 3 is a five-layered hybrid aluminum and glass-fiber-reinforced polymer (GFRP) composite [Al/0/90/0/Al]: each aluminum ply ($E = 72$ GPa and $\nu = 0.33$) is 0.38 mm thick, and each GFRP ply is 0.08 mm thick and possesses the following elastic properties: $E_L/E_T = 3.5$, $G_{LT}/E_T = 0.4$, $G_{TT}/E_T = 0.36$, $\nu_{LT} = 0.25$, and $\nu_{TT} = 0.39$, with $E_T = 13$ GPa.

A. Bending of Laminated Plates

Preliminary results are reported concerning the bending of simply supported composite plates in order to introduce the capabilities of the employed variable-kinematics modeling technique. Several 2-D models are assessed in Table 1 against the exact 3-D solution given by Pagano [48]. With reference to the coordinate axes in Fig. 2 the following nondimensionalization has been used:

$$\bar{w} = \frac{100E_T}{p_0S^4h}u_3(a/2, b/2, 0); \qquad \bar{\sigma}_{xx} = \frac{h}{p_0S^2}\sigma_{xx}(a/2, b/2, h/2)$$

$$\bar{\sigma}_{xz} = \frac{1}{p_0S}\sigma_{xz}(0, b/2, 0)$$

where $S = a/h$ is the aspect ratio and p_0 is the amplitude of the applied pressure load. All stress components are evaluated via Hooke's law except the transverse stresses of partially mixed models that come out directly as model variables.

The results in Table 1 show that the most accurate classical and advanced models LD4 and LM4 accurately recover the exact 3-D solution even for a very thick plate (aspect ratio $a/h = 4$). This feature has been confirmed within more extensive analyses concerning the linear static and free-vibration analysis of laminated plates and shells and reported in the already cited references.

B. Buckling of Laminated Plates

A verification of the present models is proposed in Table 2 by a comparison between two different ways of imposing the axial load: i.e., via a uniform strain or a uniform stress state. These will be

Table 1 Nondimensionalized bending response of rectangular plates ($b = 3a$, material 1): comparison between selected 2-D models and the exact 3-D solution of Pagano [48] for different aspect ratios a/h

	$a/h = 4$			$a/h = 50$		
	$\bar{w}$	$\bar{\sigma}_{xx}$	$\bar{\sigma}_{xz}$	$\bar{w}$	$\bar{\sigma}_{xx}$	$\bar{\sigma}_{xz}$
3-D [48]	2.82	1.14	0.351	0.520	0.628	0.439
Advanced RMVT models						
LM4	2.82	1.14	0.351	0.520	0.628	0.439
LM2	2.81	1.14	0.326	0.520	0.628	0.430
LM1	2.73	1.03	0.347	0.520	0.628	0.438
EMZ4	2.81	1.15	0.357	0.520	0.628	0.445
EMZ2	2.74	0.99	0.356	0.517	0.626	0.468
EM4	2.66	1.12	0.298	0.518	0.627	0.335
EM2	2.07	0.64	0.138	0.514	0.623	0.141
EM1	2.15	0.61	0.209	0.512	0.623	0.211
Classical PVD models						
LD4	2.82	1.14	0.351	0.520	0.628	0.439
LD2	2.80	1.13	0.347	0.520	0.628	0.438
LD1	2.72	1.01	0.353	0.519	0.627	0.438
EDZ4	2.81	1.15	0.354	0.520	0.628	0.445
EDZ2	2.74	0.98	0.353	0.517	0.626	0.438
ED4	2.62	1.11	0.278	0.518	0.627	0.313
ED2	2.04	0.64	0.156	0.513	0.623	0.159
ED1	2.05	0.61	0.157	0.511	0.623	0.158
FSDT	2.36	0.61	0.157	0.515	0.623	0.158

Table 2 Nondimensionalized uniaxial buckling load $\bar{N} = N_{cr}b^2/(E_T h^3)$ of a square symmetric laminate ($a/h = 10$, $\chi = 0$, material 2 with $N_l = 3$ and $E_L/E_T = 20$): verification of most accurate advanced and classical models for different prebuckling stress states ($\bar{N}^\epsilon$ for a uniform strain and $\bar{N}^\sigma$ for a uniform stress)

	$\bar{N}^\epsilon$	$\bar{N}^\sigma$
3-D [47]	15.0191	——
LM4	15.0196	15.1076
EMZ4	15.0485	15.1329
EM4	15.0498	15.1372
LD4	15.0196	15.1076
EDZ4	15.0508	15.1351
ED4	15.0512	15.1386
FSDT	15.0586	15.1759
CLPT	19.1827	19.3934

indicated by the superscript ϵ and σ, respectively. The 3-D elasticity solution of Noor [47] is based on the formulation of Srinivas and Rao [45] that employs a uniform strain state. The results in Table 2 refer to the full nonlinear strain definition given in Eq. (6), which conforms to the 3-D elasticity formulation. The most accurate layerwise models LM4 and LD4 both yield identical values that practically coincide with the 3-D elasticity result. Higher critical buckling loads are obtained if the axial load is referred to a uniform stress state. Constant strain in fact requires higher σ^0 values in Eq. (4), and hence smaller critical loads are obtained. This trend holds irrespective of the employed model. The most accurate classical and advanced ESL models with $N = 4$ are reported in order to show a first assessment of the proposed hierarchic modeling technique. One notes the higher accuracy obtained with advanced models. The comparison between E{M, D}4 and E{M, D}Z4 indicates that the use of MZZF has a positive influence on the accuracy of the results.

The role of von Kàrmàn's approximation is assessed in Table 3, in which classical higher-order ($N = 4$) and linear ($N = 1$) models are compared for a thick and a thin plate. Higher buckling loads are predicted by models employing von Kàrmàn's approximation: the discrepancy ranges between 2 and 2.7% for the thick-plate case and is practically negligible for the thin-plate case. The order N of the model and the type of description (ESL or LW) have a negligible influence on this discrepancy. It should be noted that von Kàrmàn's approximation is necessary to preserve the insensitivity of CLPT results to the aspect ratio of the plate. Finally, the buckling loads predicted by the linear models LD1 and ED1 are higher than those obtained with FSDT. This confirms the pathology that is peculiar to linear models retaining the full 3-D constitutive law and that has been referred to in [49] as *Poisson locking*.

Unless otherwise stated, in subsequent computations the buckling loads of the present hierarchic models will be obtained with the full nonlinear strain definition. CLPT and FSDT will refer to a uniform initial stress state to von Kàrmàn's approximation, as it is common practice in literature (see, for example, [42,47]).

Table 3 Nondimensionalized uniaxial buckling load $\bar{N} = N^\epsilon_{cr}b^2/(E_T h^3)$ of a square symmetric laminate (material 2 with $N_l = 3$ and $E_L/E_T = 20$): influence of the nonlinear contributions for a thick ($a/h = 10$) and thin plate ($a/h = 100$)

	$a/h = 10$		$a/h = 100$	
	Nonlinear strains	von Kàrmàn	Nonlinear strains	von Kàrmàn
3-D [47]	15.0191	——	——	——
LD4	15.0196	15.3127	19.6493	19.6547
LD1	15.2143	15.5145	19.6962	19.7017
ED4	15.0512	15.3440	19.6497	19.6551
ED1	15.8101	16.1310	19.9420	19.9475
FSDT	15.0586	15.3513	19.6497	19.6551
CLPT	19.1827	19.7124	19.7070	19.7124

An extensive assessment of selected 2-D plate models is presented in Table 4. The influence of the orthotropy ratio E_L/E_T and of the number of plies on the accuracy has been investigated. Present Navier solutions are compared with results available in literature, which refer to two different plate models: the layerwise model proposed in [50], which has a cubic expansion for the in-plane displacements and a quadratic one for the transverse deflection (denoted as LW_{32} in Table 4), and the third-order shear deformation theory (TSDT) proposed in [51]. One notes the excellent performance of the most accurate model LM4 for all configurations (LD4 results coincide with LM4 ones and have thus been omitted). The errors of FSDT are less than 6%; those of most higher-order models are less than 1%. The accuracy of the models decreases as the orthotropy ratio increases. If the number of layers N_l increases, the laminate tends to be quasi-isotropic and the role of the orthotropy ratio becomes less important. For low orthotropy ratios, ESL models are sufficient, whereas laminates with high orthotropy ratios require an LW description. The effectiveness of the partially mixed approach of advanced models can be clearly recognized by comparing the model pairs L{M, D}2 and E{M, D}Z4. Finally, one notes that for the considered cases it is important to retain at least a cubic order for the polynomial approximation of the displacement field. This is highlighted by the direct comparison of the model pairs EMZ{4, 3} and ED{3, 2}.

The uniaxial ($\chi = 0$) and biaxial ($\chi = 1$) buckling loads for square plates with variable aspect ratio a/h made of material 2 and material 3 are reported in Tables 5 and 6, respectively. Results of LM4 and LD4 coincide and only those of the mixed model will be reported. For coherence with the results of the preceding Section, the buckling loads for material 2 refer to a uniform strain state (superscript ϵ in Table 5), whereas the results for material 3 refer to a uniform stress state (superscript σ in Table 6) to ensure coherence with the reported FSDT and CLPT results.

A factor of 2 is seen to separate the uniaxial and the biaxial buckling loads. No difference could be appreciated in the behavior of

Table 4 Nondimensionalized uniaxial buckling load $\bar{N} = N^\epsilon_{cr}b^2/(E_T h^3)$ of a square plate ($a/h = 10$, material 2): assessment of selected 2-D models for two symmetric laminates and varying orthotropy ratio E_L/E_T

	E_L/E_T				
	3	10	20	30	40
$N_l = 3$					
3-D [47]	5.3044	9.7621	15.0191	19.3040	22.8807
LM4	5.3051	9.7628	15.0196	19.3045	22.8811
LM2	5.3061	9.7673	15.0328	19.3301	22.9220
EMZ4	5.3056	9.7704	15.0485	19.3635	22.9761
EMZ3	5.3153	9.8147	15.1674	19.5679	23.2667
LD2	5.3066	9.7710	15.0423	19.3584	22.9690
EDZ4	5.3056	9.7710	15.0508	19.3684	22.9842
ED3	5.3060	9.7720	15.0551	19.3785	23.0021
ED2	5.3556	9.9945	15.6458	20.4027	24.4816
LW_{32} [50]	5.3112	9.7961	15.0757	19.3761	22.9643
TSDT [51]	5.3933	9.9406	15.2980	19.6740	23.3400
FSDT	5.3991	9.9653	15.3513	19.7566	23.4529
CLPT	5.7538	11.4918	19.7124	27.9357	36.1597
$N_l = 9$					
3-D [47]	5.3352	10.0417	15.9153	20.9614	25.3436
LM4	5.3354	10.0419	15.9155	20.9616	25.3437
LM2	5.3354	10.0419	15.9156	20.9617	25.3439
EMZ4	5.3359	10.0469	15.9336	20.9977	25.4007
EMZ3	5.3752	10.2057	16.3588	21.7619	26.5462
LD2	5.3354	10.0420	15.9156	20.9619	25.3442
EDZ4	5.3359	10.0470	15.9338	20.9981	25.4012
ED3	5.3385	10.0578	15.9629	21.0501	25.4786
ED2	5.3810	10.2301	16.4245	21.8793	26.7207
LW_{32} [50]	5.3400	10.0572	15.9403	20.9926	25.3791
TSDT [51]	5.4313	10.1970	16.1720	21.3150	25.7900
FSDT	5.4126	10.1895	16.1459	21.2650	25.7152
CLPT	5.7538	11.4918	19.7124	27.9357	36.1597

Table 5 Nondimensionalized buckling load $\bar{N} = N^{\epsilon}_{cr} b^2/(E_T h^3)$ of symmetric cross-ply square plates (material 2 with $E_L/E_T = 25$ and $N_l = 3$)

a/h	LM4	LM2	EMZ4	EM3	EDZ4	ED4	FSDT
Uniaxial compression: $\chi = 0$ (CLPT solution: $\bar{N} = 23.8239$)							
10	17.2645	17.2835	17.3075	17.3145	17.3110	17.3127	17.6568
20	21.7142	21.7202	21.7277	21.7295	21.7288	21.7304	21.8687
25	22.4250	22.4289	22.4339	22.4351	22.4347	22.4358	22.5307
50	23.4565	23.4575	23.4588	23.4591	23.4590	23.4593	23.4855
100	23.7309	23.7311	23.7315	23.7315	23.7315	23.7316	23.7383
Biaxial compression: $\chi = 1$ (CLPT solution: $\bar{N} = 11.9120$)							
10	8.6820	8.6914	8.7010	8.7043	8.7028	8.7057	8.8284
20	10.8768	10.8798	10.8833	10.8842	10.8839	10.8849	10.9344
25	11.2260	11.2280	11.2304	11.2310	11.2308	11.2314	11.2654
50	11.7320	11.7325	11.7331	11.7333	11.7332	11.7334	11.7428
100	11.8664	11.8665	11.8667	11.8667	11.8667	11.8668	11.8692

the models' accuracy between these two loading configurations. All formulations consistently converge toward CLPT results when the plate becomes thinner. If LM4 results are taken as reference values for thick laminates, one notes that ESL models including MZZF are more accurate than those without the slope discontinuity at the interfaces. This hierarchic accuracy can be confirmed in the case of the hybrid Al-GFRP composite that is characterized by the strong mismatch between the plies' stiffnesses.

C. Buckling of Laminated Shells

1. Axially Loaded Open Cylindrical Panels

Table 7 compares the results of selected 2-D models against those obtained in [52] by means of the analytical Navier-type solution for a zigzag model. The nondimensionalized buckling loads have been reported for an axially loaded cylindrical square panel with constant length-to-radius ratio $a/R = 0.05$ and variable aspect ratio a/h. The

Table 6 Nondimensionalized buckling load $\bar{N} = N^{\sigma}_{cr} b^2/(E_{(Al)} h^3)$ of symmetric cross-ply square plates (material 3)

a/h	LM4	LM2	EMZ4	EM3	EDZ4	ED4	FSDT
Uniaxial compression: $\chi = 0$ (CLPT solution: $\bar{N} = 3.6547$)							
10	3.1066	3.1068	3.2577	3.2938	3.2613	3.3084	3.4075
20	3.4978	3.4978	3.5448	3.5563	3.5466	3.5606	3.5896
25	3.5525	3.5525	3.5836	3.5911	3.5847	3.5939	3.6128
50	3.6285	3.6285	3.6367	3.6387	3.6370	3.6394	3.6441
100	3.6481	3.6481	3.6503	3.6508	3.6504	3.6510	3.6521
Biaxial compression: $\chi = 1$ (CLPT solution: $\bar{N} = 1.8274$)							
10	1.5533	1.5534	1.6279	1.6469	1.6308	1.6542	1.7037
20	1.7489	1.7489	1.7724	1.7782	1.7731	1.7803	1.7948
25	1.7762	1.7763	1.7918	1.7955	1.7924	1.7970	1.8064
50	1.8143	1.8143	1.8184	1.8193	1.8185	1.8197	1.8221
100	1.8241	1.8241	1.8251	1.8254	1.8252	1.8255	1.8260

Table 7 Nondimensionalized buckling load $\bar{N} = N^{\sigma}_{cr} a^2/(E_T h^3)$ of an axially loaded cylindrical panel with $a/R = 0.05$ and variable aspect ratio a/h (material 2 with $E_L/E_T = 40$, $N_l = 5$, and $h_k = h/N_l$, and buckling mode $m = n = 1$)

	a/h				
	10	20	30	50	100
[52]	24.19	31.91	34.04	35.42	36.86
LM4	23.98	31.86	34.02	35.41	36.84
LD2	23.99	31.86	34.02	35.41	36.84
LM1	24.09	31.90	34.04	35.42	36.85
EMZ4	24.17	31.93	34.06	35.42	36.85
EDZ4	24.17	31.93	34.06	35.42	36.85
ED4	24.20	31.94	34.06	35.42	36.85
ED3	24.20	31.94	34.06	35.42	36.85
ED2	25.27	32.37	34.27	35.50	36.87
FSDT	24.18	31.90	34.04	35.42	36.85
CLPT	35.84	35.87	35.94	36.13	37.03

consistency of the results is highlighted, with the most accurate LW descriptions being more accurate than the advanced zigzag models. These differences decrease as the aspect ratio increases. Note that the curvature terms make the CLPT solution dependent on the aspect ratio a/h.

The combined effect of length-to-radius ratio a/R and aspect ratio a/h of square cylindrical panels is analyzed in Table 8 (same laminate as in Table 7). Except where explicitly indicated by the superscripts a, b, and c, the buckling mode corresponds to the number of half-waves $m = 1$ and $n = 1$. FSDT_{nl} relies on the full nonlinear strain definition; i.e., von Kàrmàn's approximation has been discarded. Furthermore, Table 8 reports the buckling loads obtained with the most accurate model LM4_{Δ} and the classical model FSDT_{Δ} by retaining Donnell's shallow shell approximation (subscript Δ). Because of previous results, LM4 results will be taken as reference values. All models correctly show that the buckling load increases as the curvature of the shell increases (i.e., as the ratio a/R increases). The accuracy of the considered higher-order models appear to be predominantly affected by the aspect ratio a/h and less dependent on curvature effects. However, the accuracy of FSDT is degraded for highly curved shells when von Kàrmàn's nonlinearities are used. Further improvements of FSDT results are expected when adapted shear correction factors are used (we recall that a shear correction factor of $\kappa^2 = 5/6$ is employed throughout this paper, irrespective of the laminate). As expected, Donnell's approximation lead to larger discrepancies (higher buckling loads) for increasing curvature and is insensitive to the aspect ratio of the panel. Note that different buckling modes may be predicted by using Donnell's approximation. In the present case, this occurs for the rather thin panel with $a/h = 50$ and $a/R = 2$.

2. Laminated Hollow Cylinders

Since in a closed hollow cylinder the deformation pattern in the circumferential direction is always characterized by full waves, we shall refer in the following to the integer mode number $n' = n/2$ with $n = 2, 4, \ldots$. An assessment of selected higher-order 2-D models against 3-D solutions available in literature is presented in Table 9 for an unsymmetrically laminated, specially orthotropic hollow cylinder with $N_l = 40$. Even if, as discussed in the Introduction, the application of the linearized buckling analysis to unsymmetric laminates is questionable, this example has been retained, since various 3-D solutions are available in open literature. The 3-D solution in [53] refers to a pure axial prestress, whereas the 3-D solution in [46] retains a full 3-D prebuckling stress state with $\sigma^0_{zz} \neq 0$. Note that the cited results do not permit associating a lower bound for the buckling load with either prestress state. Present results obtained with the most accurate advanced model LM4 are shown to exactly match the 3-D solution in [53]. An assessment of selected 2-D models shows that all models correctly associate the lowest buckling load with the mode $m = 3$ and $n' = 2$. Furthermore, for a given laminate and geometry, the errors due to 2-D approximations are shown to depend on the number of axial and circumferential waves of the mode. However, for the considered quasi-isotropic

Table 8 Nondimensionalized buckling load $\bar{N} = N^{\sigma}_{cr}a^2/(E_T h^3)$ of axially loaded square cylindrical panels with various curvature-to-length ratios R/a and length-to-thickness ratios a/h (material as in Table 7) and buckling mode $m = n = 1$, except where explicitly indicated (subscript Δ indicates use of Donnell's approximation)

	a/h							
	10	20	50	100	10	20	50	100
	$a/R = 0.1$				$a/R = 0.2$			
LM4	23.99	31.97	36.27	40.42	24.02	32.40	39.72	54.67
LD2	23.99	31.97	36.27	40.42	24.03	32.40	39.72	54.67
EMZ4	24.18	32.04	36.29	40.42	24.21	32.48	39.73	54.67
ED4	24.20	32.05	36.29	40.42	24.23	32.49	39.74	54.67
FSDT	24.21	32.04	36.31	40.46	24.31	32.57	39.88	54.88
$FSDT_{nl}$	23.97	31.90	36.25	40.41	24.00	32.33	39.70	54.67
$LM4_{\Delta}$	24.00	31.98	36.29	40.43	24.08	32.46	39.79	54.74
$FSDT_{\Delta}$	24.22	32.05	36.33	40.48	24.37	32.63	39.95	54.95
	$a/R = 1$				$a/R = 2$			
LM4	25.08	45.21	140.6	253.3[a]	28.12	74.92	219.8[b]	447.9[c]
LD2	25.08	45.21	140.6	253.3[a]	28.12	74.92	219.8[b]	447.9[c]
EMZ4	25.24	45.27	140.6	253.3[a]	28.21	74.96	220.1[b]	448.2[c]
ED4	25.26	45.28	140.6	253.3[a]	28.23	74.97	220.1[b]	448.2[c]
FSDT	27.63	49.61	154.1	259.4[a]	38.90	103.9	243.7[b]	469.1[c]
$FSDT_{nl}$	25.03	45.14	140.6	253.2[a]	27.96	74.84	221.3[b]	448.9[c]
$LM4_{\Delta}$	26.19	46.56	142.0	254.9[a]	30.98	78.45	230.7[a]	461.0[c]
$FSDT_{\Delta}$	28.99	51.16	155.8	261.1[a]	43.43	109.1	253.3[a]	483.2[c]

[a]Buckling modes: $m = 2$ and $n = 2$.
[b]Buckling modes: $m = 1$ and $n = 2$.
[c]Buckling modes: $m = 2$ and $n = 3$.

laminate, the maximum error of the ED2 model is about 6% for the mode $m = 3$ and $n' = 3$.

The influence of the orthotropy ratio is analyzed in Table 10 for two symmetric stacking sequences made of four and eight layers of material 2. Present results are compared against 3-D results extracted from the graphics in [46]. A good agreement between the results is obtained, with the discrepancies being attributed to the different definition of the prebuckling stress state (it is recalled that a 3-D initial stress state is used in [46]). In particular, the critical buckling load of both considered laminates has been found to occur for the same number of axial and circumferential half-waves $(m, n = 2n')$ as that reported in [46]. As expected, the errors of less accurate 2-D models increase as the orthotropy ratio increases. For $E_L/E_T = 40$ the largest error of the ED2 model is of about 5%. If FSDT is used with von Kàrmàn's approximation, one finds errors of about 25% even for low orthotropy ratios. The use of full nonlinearities is thus recommended in conjunction with FSDT for closed hollow cylinders. Finally, it is interesting to note that for the $[0/90]_s$ laminate, the advanced higher-order ESL model EMZ4 predicts slightly lower buckling loads compared to the classical LW model LD2, whereas the opposite is true for the $[0/90/0/90]_s$ laminate.

The effect of cylinder geometry is finally addressed by analyzing the buckling loads of hollow tubes with various length-to-radius ratios a/R and different thickness-to-radius ratios h/R. The hybrid Al-GFRP laminate of material 3 has been taken for this example. Following [54], we report the results in terms of the slenderness ratio $(a/R)/(R/h)^{1/2}$. It is expected that the solution for large a/R comes close to Euler's global buckling load and that for short rings one recovers the typical flat-plate-strip behavior [20,54]. Euler's global buckling load is evaluated as $P^E_{cr} = A^{\star} I(\pi/a)^2$, where I is the moment of inertia and $A^{\star} = A_{11}A_{22} - A^2_{12}/(A_{22}A_{66}h)$ is computed from the reduced constitutive coefficients $C^{\star}_{pq}$ $[p, q \in (1, 6)]$ [55]. The buckling load of a flat-plate strip is defined according to CLPT as $P^P_{cr} = \pi^2 D^{\star}/a^2$, where $D^{\star}$ is the bending stiffness of the plate computed as [42]

$$D^{\star} = \int_h C^{\star}_{11} z^2 \, dz$$

The results in Table 11 confirm that the buckling loads of long cylinders can be well estimated by the simple Euler's column buckling formula. Note that the convergence toward Euler's column buckling load depends on the ratio h/R. For small values of the slenderness parameter $(a/R)/(R/h)^{1/2}$, the buckling modes show a more complex deformation pattern and the solution typically depends on the effects of curvature and laminate thickness. Except for small values of the slenderness parameter of the cylinder with large thickness-to-radius ratio $(h/R = 2)$, the role of shear deformation and transverse normal stresses appears to be negligible. Finally, the FSDT and CLPT results obtained with von Kàrmàn's approximation (not reported in Table 11) are much less accurate, even in the case of slender cylinders.

Table 9 Nondimensionalized buckling load $\bar{N} = N^{\sigma}_{cr}R^2/(E_T h^3)$ of an axially loaded hollow cylinder: $a/R = 5$, $h/R = 0.2$ (40-layered $[0/90]_{20}$ laminate (fibers are in circumferential direction in the outer ply) with following lamina properties: $E_L/E_T = 15$, $G_{LT}/E_T = 0.5$, $G_{TT}/E_T = 0.35$, and $\nu_{LT} = \nu_{TT} = 0.3$); number representation is $0.1234^{+5} = 0.1234 \times 10^5$

m	n'	3-D [53]	3-D [46]	LM4	EMZ4	ED4	ED2
1	1	0.5511^{+1}	0.5520^{+1}	0.5511^{+1}	0.5511^{+1}	0.5511^{+1}	0.5512^{+1}
1	2	0.1108^{+2}	0.1110^{+2}	0.1108^{+2}	0.1110^{+2}	0.1115^{+2}	0.1155^{+2}
1	3	0.5770^{+2}	0.5758^{+2}	0.5770^{+2}	0.5789^{+2}	0.5844^{+2}	0.6246^{+2}
2	1	0.6380^{+1}	0.6391^{+1}	0.6380^{+1}	0.6381^{+1}	0.6382^{+1}	0.6391^{+1}
2	2	0.5466^{+1}	0.5467^{+1}	0.5467^{+1}	0.5472^{+1}	0.5489^{+1}	0.5614^{+1}
2	3	0.1654^{+2}	0.1667^{+2}	0.1654^{+2}	0.1659^{+2}	0.1673^{+2}	0.1779^{+2}
3	1	0.6838^{+1}	0.6849^{+1}	0.6838^{+1}	0.6839^{+1}	0.6845^{+1}	0.6880^{+1}
3	2	0.5052^{+1}	0.5051^{+1}	0.5052^{+1}	0.5056^{+1}	0.5073^{+1}	0.5187^{+1}
3	3	0.9622^{+1}	0.9613^{+1}	0.9622^{+1}	0.9647^{+1}	0.9726^{+1}	0.1028^{+2}

Table 10 Nondimensionalized buckling load $\bar{N} = N^{\sigma}_{cr}/(E_T h)$ of an axially loaded hollow cylinder with $h/R = 0.2$ and $a/R = 5$: results for two symmetric stacking sequences of material 2 with varying orthotropy ratio E_L/E_T

	E_L/E_T				
	5	10	20	30	40
	$[0/90]_s$ $(m = 2, n' = 2)$				
[46]	0.142	0.177	0.230	0.272	0.305
LM4	0.1377	0.1757	0.2275	0.2667	0.2992
LD2	0.1377	0.1759	0.2282	0.2681	0.3014
EMZ4	0.1377	0.1759	0.2281	0.2679	0.3011
ED4	0.1377	0.1758	0.2282	0.2682	0.3016
ED2	0.1385	0.1778	0.2330	0.2767	0.3144
$FSDT_{nl}$	0.1385	0.1770	0.2305	0.2721	0.3075
FSDT	0.1735	0.2211	0.2880	0.3401	0.3844
	$[0/90/0/90]_s$ $(m = 3, n' = 2)$				
[46]	0.147	0.193	0.260	0.308	0.346
LM4	0.1581	0.2005	0.2601	0.3042	0.3393
LD2	0.1581	0.2005	0.2601	0.3043	0.3393
EMZ4	0.1581	0.2006	0.2605	0.3049	0.3403
ED4	0.1581	0.2007	0.2607	0.3054	0.3410
ED2	0.1592	0.2033	0.2671	0.3161	0.3561
$FSDT_{nl}$	0.1586	0.2012	0.2614	0.3064	0.3425
FSDT	0.1939	0.2480	0.3245	0.3813	0.4268

The behavior for small slenderness ratios is reported in Table 12 for two cylinders with $h/R = 0.02$ and $h/R = 0.002$. The buckling load predicted by the simple flat-plate-strip approach is seen to correspond to the critical load of cylinders whose slenderness ratio approximately equals the h/R ratio: i.e., when the ratio $(a/R) \times (R/h)^{1/2} \approx 1$ [54]. For larger values of the slenderness ratio, the typical cylinder response is obtained and the critical loads are strongly dependent on the buckling modes. For these geometries, 2-D approximations have a moderate impact on the buckling load. For very short rings with $(a/R) \times (R/h)^{1/2} < 1$ the 2-D approximations become more important with discrepancies that depend on the aspect ratio a/h. Note that the aspect ratio a/h of the cylinder with $(a/R) \times (R/h)^{1/2} = 0.1$ is less than one, so that plate approximation is meaningless. In this case, transverse shear deformation is known to play a major role [54].

Therefore, the results in Table 11 and 12 confirm the following:

1) Slender cylinders present a global buckling behavior, for which the classical Euler column buckling formula can be used.

2) Short rings with $(a/R) \times (R/h)^{1/2} \approx 1$ do have a typical flat-plate behavior, for which the findings of Sec. III.B can be applied.

Table 11 Nondimensionalized buckling load $\bar{N} = N^{\sigma}_{cr}a^2/(E_T R^2 h)$ of axially loaded hollow cylinders: influence of cylinder geometry (material 3)

	Slenderness ratio $(a/R)/\sqrt{R/h}$				
	1	2	5	10	20
	$h/R = 0.02$, $\bar{P}^E_{cr} = 4.388$				
(m, n')	(1, 2)	(1, 2)	(1, 1)	(1, 1)	(1, 1)
LM4	0.458	1.521	4.235	4.312	4.331
EMZ4	0.458	1.522	4.236	4.312	4.332
ED4	0.458	1.522	4.237	4.314	4.333
ED2	0.458	1.522	4.237	4.314	4.334
$FSDT_{nl}$	0.459	1.525	4.235	4.312	4.331
$CLPT_{nl}$	0.459	1.525	4.235	4.312	4.331
	$h/R = 0.2$, $\bar{P}^E_{cr} = 4.381$				
(m, n')	(1, 2)	(2, 2)	(1, 1)	(1, 1)	(1, 1)
LM4	0.326	1.307	3.546	4.137	4.321
EMZ4	0.335	1.339	3.547	4.138	4.322
ED4	0.338	1.351	3.548	4.139	4.323
ED2	0.343	1.370	3.548	4.139	4.323
$FSDT_{nl}$	0.345	1.380	3.548	4.139	4.323
$CLPT_{nl}$	0.359	1.435	3.548	4.139	4.323

Table 12 Nondimensionalized buckling load $\bar{N} = N^{\sigma}_{cr}a^2/(E_T h^3)$ of axially loaded hollow cylinders: influence of cylinder geometry (material 3) (number representation is as in Table 9

	Slenderness ratio $(a/R)/\sqrt{R/h}$				
	0.2	0.1	0.02	0.01	0.002
	$h/R = 0.02$, $\bar{P}^P_{cr} = 0.9173^{+0}$				
(m, n')	(1,5)	(2,6)	(1,1)	(1,1)	(1,1)
LM4	0.5177^{+2}	0.1325^{+2}	0.8653^{+0}	0.5552^{+0}	0.8195^{-1}
LM4	0.5177^{+2}	0.1325^{+2}	0.8653^{+0}	0.5552^{+0}	0.8195^{-1}
EMZ4	0.5187^{+2}	0.1335^{+2}	0.9039^{+0}	0.6309^{+0}	0.9364^{-1}
ED4	0.5191^{+2}	0.1338^{+2}	0.9158^{+0}	0.6573^{+0}	0.9838^{-1}
ED2	0.5196^{+2}	0.1342^{+2}	0.9367^{+0}	0.7095^{+0}	0.1206^{+0}
$FSDT_{nl}$	0.5203^{+2}	0.1342^{+2}	0.9291^{+0}	0.6887^{+0}	0.1077^{+0}
$CLPT_{nl}$	0.5216^{+2}	0.1354^{+2}	0.9887^{+0}	0.8662^{+0}	0.1515^{+0}
FSDT	0.5438^{+2}	0.1361^{+2}	0.9427^{+0}	0.7162^{+0}	0.1108^{+0}
CLPT	0.5452^{+2}	0.1374^{+2}	0.1005^{+1}	0.9233^{+0}	0.9173^{+0}
	$h/R = 0.002$, $\bar{P}^P_{cr} = 0.9173^{+0}$				
(m, n')	(1, 5)	(1, 7)	(2, 6)	(3, 1)	(1, 1)
LM4	0.5344^{+4}	0.1380^{+4}	0.1543^{+3}	0.1415^{+2}	0.9868^{+0}
EMZ4	0.5345^{+4}	0.1381^{+4}	0.1543^{+3}	0.1417^{+2}	0.9920^{+0}
ED4	0.5346^{+4}	0.1381^{+4}	0.1543^{+3}	0.1417^{+2}	0.9934^{+0}
ED2	0.5346^{+4}	0.1381^{+4}	0.1543^{+3}	0.1418^{+2}	$0.9959(^{+0}$
$FSDT_{nl}$	0.5345^{+4}	0.1381^{+4}	0.1543^{+3}	0.1417^{+2}	0.9950^{+0}
$CLPT_{nl}$	0.5345^{+4}	0.1381^{+4}	0.1543^{+3}	0.1420^{+2}	0.1002^{+1}
FSDT	0.5565^{+4}	0.1410^{+4}	0.1548^{+3}	0.1418^{+2}	0.9966^{+0}
CLPT	0.5565^{+4}	0.1410^{+4}	0.1548^{+3}	0.1421^{+2}	0.1003^{+1}

In these cases, the buckling loads predicted by the linearized stability analysis can be effectively used. For all intermediate values of the slenderness parameter, however, the typical cylinder behavior is obtained, for which the validity of the linearized stability analysis is limited as discussed in Sec. I. In these cases, a full nonlinear analysis and stability investigation is necessary, or a lower bound for the critical load should be devised by means of appropriate knockdown factors.

IV. Conclusions

The paper has extended variable-kinematics models based on Carrera's unified formulation to the linearized buckling analysis of laminated plates and shells. Governing stability equations have been derived in the case of double curved shells loaded by in-plane compression. The von Kàrmàn and exact nonlinear strain-displacement relations have been accounted for, along with preloads corresponding to both a constant-strain and a constant-stress state. The effect of higher-order terms, layerwise description, and mixed assumptions have been analyzed for a large number of plate/shell problems. The following main conclusions can be drawn. Higher-order, layerwise, and mixed results reduce to classical Kirchhoff–Love type theories in the case of thin-plate/shell structures. Errors with respect to 3-D solution can be reduced to a great extent by the use of higher-order theories in the case of moderately thick laminated plates/shells. Three-dimensional buckling results are obtained by using the most accurate layerwise solutions in the case of thick structures. Finally, buckling loads corresponding to a constant-strain state are lower than those related to constant-stress hypothesis. Future work could be directed toward the finite element implementation of the proposed theories and to their use in geometrically nonlinear analyses.

Appendix: Fundamental Nuclei for the Geometric Stiffness Matrix

This Appendix reports the expressions of the 3×3 fundamental nuclei of the geometric stiffness matrix $\mathbf{K}$ for the initial stress and initial strain formulations. In either case, the following integrals over the layer's thickness h_k are introduced:

$$\{J^{k\tau s}_{\beta/\alpha}, J^{k\tau s}_{\alpha/\beta}\} = \int_{h_k} F_\tau(z) F_s(z) \left\{ \frac{H_{\beta_k}}{H_{\alpha_k}}, \frac{H_{\alpha_k}}{H_{\beta_k}} \right\} \mathrm{d}z \qquad \text{(A1)}$$

Furthermore, two tracers δ_{vK} and δ_D will be used to introduce von Kàrmàn's and Donnell's approximations, respectively, into the expression of the nonlinear terms of the strain field by setting them to zero.

In the following, the subscript (mn) of Eq. (10) can be omitted without loss of clarity. For the formulation of the prebuckling state in terms of a uniform (unitary) compressive stress $\sigma^0_{\alpha_k\alpha_k} = -1$, the nonzero terms of the fundamental nucleus $\mathbf{K}^{k\tau s}_{\sigma}$ for the most general case of a doubly curved shell under a biaxial in-plane load read as follows:

$$
\begin{aligned}
&\mathbf{K}^{k\tau s}_{\sigma}(1,1) = -\delta_{vK}[J^{k\tau s}_{\beta/\alpha}(m^2 + \delta_D R^{-2}_{\alpha_k}) + \chi J^{k\tau s}_{\alpha/\beta} n^2];\\
&\mathbf{K}^{k\tau s}_{\sigma}(1,3) = \delta_D \delta_{vK} J^{k\tau s}_{\beta/\alpha} R^{-1}_{\alpha_k} m;\\
&\mathbf{K}^{k\tau s}_{\sigma}(2,2) = -\delta_{vK}[J^{k\tau s}_{\beta/\alpha} m^2 + \chi J^{k\tau s}_{\alpha/\beta}(n^2 + \delta_D R^{-2}_{\beta_k})];\\
&\mathbf{K}^{k\tau s}_{\sigma}(2,3) = \delta_D \delta_{vK} \chi J^{k\tau s}_{\alpha/\beta} R^{-1}_{\beta_k} n; \qquad \mathbf{K}^{k\tau s}_{\sigma}(3,1) = \mathbf{K}^{k\tau s}_{\sigma}(1,3);\\
&\mathbf{K}^{k\tau s}_{\sigma}(3,2) = \mathbf{K}^{k\tau s}_{\sigma}(2,3);\\
&\mathbf{K}^{k\tau s}_{\sigma}(3,3) = -J^{k\tau s}_{\beta/\alpha}(m^2 + \delta_D \delta_{vK} R^{-2}_{\alpha_k}) - \chi J^{k\tau s}_{\alpha/\beta}(n^2 + \delta_D \delta_{vK} R^{-2}_{\beta_k})
\end{aligned}
\tag{A2}
$$

If the prebuckling state is given by a uniform (unitary) compressive strain $\epsilon^0_{\alpha_k\alpha_k} = -1$, the terms of the fundamental nucleus $\mathbf{K}^{k\tau s}_{\sigma}$ have the following expression:

$$
\begin{aligned}
&\mathbf{K}^{k\tau s}_{\sigma}(1,1) = -\delta_{vK}[\tilde{C}^k_{11} J^{k\tau s}_{\beta/\alpha}(m^2 + \delta_D R^{-2}_{\alpha_k}) + \chi \tilde{C}^k_{22} J^{k\tau s}_{\alpha/\beta} n^2];\\
&\mathbf{K}^{k\tau s}_{\sigma}(1,3) = \delta_D \delta_{vK} \tilde{C}^k_{11} J^{k\tau s}_{\beta/\alpha} R^{-1}_{\alpha_k} m;\\
&\mathbf{K}^{k\tau s}_{\sigma}(2,2) = -\delta_{vK}[\tilde{C}^k_{11} J^{k\tau s}_{\beta/\alpha} m^2 + \chi \tilde{C}^k_{22} J^{k\tau s}_{\alpha/\beta}(n^2 + \delta_D R^{-2}_{\beta_k})];\\
&\mathbf{K}^{k\tau s}_{\sigma}(2,3) = \delta_D \delta_{vK} \chi \tilde{C}^k_{22} J^{k\tau s}_{\alpha/\beta} R^{-1}_{\beta_k} n; \qquad \mathbf{K}^{k\tau s}_{\sigma}(3,1) = \mathbf{K}^{k\tau s}_{\sigma}(1,3);\\
&\mathbf{K}^{k\tau s}_{\sigma}(3,2) = \mathbf{K}^{k\tau s}_{\sigma}(2,3);\\
&\mathbf{K}^{k\tau s}_{\sigma}(3,3) = -\tilde{C}^k_{11} J^{k\tau s}_{\beta/\alpha}(m^2 + \delta_D \delta_{vK} R^{-2}_{\alpha_k})\\
&\quad - \chi \tilde{C}^k_{22} J^{k\tau s}_{\alpha/\beta}(n^2 + \delta_D \delta_{vK} R^{-2}_{\beta_k})
\end{aligned}
\tag{A3}
$$

For cylindrical shells (open or closed) under pure axial loading, the above expressions are simplified by setting $\chi = 0$, $R_{\beta_k} = R^k$ and $R_{\alpha_k} = 0$, which leads to the following nonzero contributions of $\mathbf{K}^{k\tau s}_{\sigma}$:

$$
\mathbf{K}^{k\tau s}_{\sigma}(1,1) = \mathbf{K}^{k\tau s}_{\sigma}(2,2) = -\delta_{vK} J^{k\tau s}_{\beta} m^2 \qquad \mathbf{K}^{k\tau s}_{\sigma}(3,3) = -J^{k\tau s}_{\beta} m^2 \tag{A4}
$$

The geometric stiffness matrix for plate geometries is obtained by further setting $R_{\beta_k} = 0$. By retaining the biaxial load ratio χ, the nonzero terms of the fundamental nucleus for a stress-driven prebuckling deformation in this case are

$$
\begin{aligned}
&\mathbf{K}^{k\tau s}_{\sigma}(1,1) = \mathbf{K}^{k\tau s}_{\sigma}(2,2) = -\delta_{vK} J^{k\tau s}(m^2 + \chi n^2);\\
&\mathbf{K}^{k\tau s}_{\sigma}(3,3) = -J^{k\tau s}(m^2 + \chi n^2)
\end{aligned}
\tag{A5}
$$

with $J^{k\tau s}$ defined by Eq. (A1) with $H_{\alpha_k} = H_{\beta_k} = 1$. Similar expressions are easily derived for a strain-driven prebuckling state from Eq. (A3).

References

[1] Riks, E., "Buckling," *Encyclopedia of Computational Mechanics*, edited by E. Stein, R. de Borst, and T. J. R. Hughes, Vol. 2, Wiley, New York, 2004.

[2] Bushnell, D., *Computerized Buckling Analysis of Shells*, M. Nihhoff, Dordrecht, The Netherlands, 1985.

[3] Elishakoff, I., van Manen, S., Vermeulen, P. G., and Arbocz, J., "First-Order Second-Moment Analysis of the Buckling of Shells with Random Imperfections," *AIAA Journal*, Vol. 25, 1987, pp. 1113–1117. doi:10.2514/3.9751

[4] Timoshenko, S. P., and Gere, J. M., *Theory of Elastic Stability*, McGraw–Hill, New York, 1961.

[5] Jabareen, M., "Rigorous Buckling of Laminated Cylindrical Shells," *Thin-Walled Structures*, Vol. 47, 2009, pp. 233–240. doi:10.1016/j.tws.2008.05.009

[6] "Buckling of Structures," *European Cooperation for Space Standardization*, ESA, European Space Research and Technology Centre, Noordwijk, The Netherlands, 2010.

[7] Anonymous, "Buckling of Thin-Walled Circular Cylinders," NASA Space Vehicle Design Criteria NASA SP-8007, NASA, 1968.

[8] Arbocz, J., and Starnes, J. H., Jr, "Future Directions and Challenges in Shell Stability Analysis," *Thin-Walled Structures*, Vol. 40, 2002, pp. 729–754. doi:10.1016/S0263-8231(02)00024-1

[9] Arbocz, J., and Hilburger, M. W., "Toward a Probabilistic Preliminary Design Criterion for Buckling Critical Composite Shells," *AIAA Journal*, Vol. 43, 2005, pp. 1823–1827. doi:10.2514/1.11368

[10] Hilburger, M. W., and Starnes, J. H., Jr., "Effect of Imperfections on the Buckling Response of Compression-Loaded Composite Shells," *International Journal of Non-Linear Mechanics*, Vol. 37, 2002, pp. 623–643. doi:10.1016/S0020-7462(01)00088-9

[11] Leissa, A. W., "Conditions for Laminated Plates to Remain Flat Under Inplane Loading," *Composite Structures*, Vol. 6, 1986, pp. 261–270. doi:10.1016/0263-8223(86)90022-X

[12] Singh, G., Rao, G. V., and Iyengar, N. G. R., "Bifurcation Buckling of Unsymmetrically Laminated Plates," *Composites Engineering*, Vol. 4, 1994, pp. 181–194. doi:10.1016/0961-9526(94)90026-4

[13] Hilburger, M. W., Nemeth, M. P., and Starnes, J. H., Jr., "Shell Buckling Design Criteria Based on Manufacturing Imperfection Signatures," *AIAA Journal*, Vol. 44, 2006, pp. 654–663. doi:10.2514/1.5429

[14] Kapania, R. K., "A Review on the Analysis of Laminated Shells," *Journal of Pressure Vessel Technology*, Vol. 111, 1989, pp. 89–96.

[15] Noor, A. K., and Burton, W. S., "Assessment of Computational Models for Multilayered Composite Shells," *Applied Mechanics Reviews*, Vol. 43, 1990, pp. 67–97.

[16] Carrera, E., "Historical Review of Zig-Zag Theories for Multilayered Plates and Shells," *Applied Mechanics Reviews*, Vol. 56, 2003, pp. 287–308. doi:10.1115/1.1557614

[17] Carrera, E., "Theories and Finite Elements for Multilayered, Anisotropic, Composite Plates and Shells," *Archives of Computational Methods in Engineering*, Vol. 9, 2002, pp. 87–140. doi:10.1007/BF02736649

[18] Leissa, A. W., "An Overview of Composite Plate Buckling," *Proceedings of the 4th International Conference on Composite Structures*, Vol. 1, Elsevier, London, 1987, pp. 1–29.

[19] Kapania, R. K., and Raciti, S., "Recent Advances in Analysis of Laminated Beams and Plates, Part 1: Shear Effects and Buckling," *AIAA Journal*, Vol. 27, 1989, pp. 923–934. doi:10.2514/3.10202

[20] Carrera, E., "The Effects of Shear Deformation and Curvature on Buckling and Vibrations of Cross-Ply Laminated Composite Shells," *Journal of Sound and Vibration*, Vol. 150, 1991, pp. 405–433. doi:10.1016/0022-460X(91)90895-Q

[21] Weaver, P. M., "Anisotropy-Induced Spiral Buckling in Compression Loaded Cylindrical Shells," *AIAA Journal*, Vol. 40, 2002, pp. 1001–1007. doi:10.2514/2.1740

[22] Weaver, P. M., Driesen, J. R., and Roberts, P., "The Effect of Flexural/Twist Anisotropy on Compression Buckling of Quasi-Isotropic Laminated Cylindrical Shells," *Composite Structures*, Vol. 55, 2002, pp. 195–204. doi:10.1016/S0263-8223(01)00147-7

[23] Ji, W., and Waas, A. M., "Wrinkling and Edge Buckling in Orthotropic Sandwich Beams," *Journal of Engineering Mechanics*, Vol. 134, 2008, pp. 455–461. doi:10.1061/(ASCE)0733-9399(2008)134:6(455)

[24] Jaunky, N., and Knight, N. F., "An Assessment of Shell Theories for Buckling of Circular Cylindrical Laminated Composite Panels Loaded in Axial Compression," *International Journal of Solids and Structures*, Vol. 36, 1999, pp. 3799–3820. doi:10.1016/S0020-7683(98)00177-2

[25] Wong, K. F. W., and Weaver, P. M., "Approximate Solution for the Compression Buckling of Fully Anisotropic Cylindrical Shells," *AIAA Journal*, Vol. 43, 2005, pp. 2639–2645. doi:10.2514/1.10924

[26] Carrera, E., "A Class of Two Dimensional Theories for Multilayered Plates Analysis," *Atti dell'Accademia delle Scienze di Torino, Memorie Scienze Fisiche*, Vols. 19–20, 1995, pp. 49–87.

[27] Carrera, E., "Theories and Finite Elements for Multilayered Plates and Shells: A Unified Compact Formulation with Numerical Assessment and Benchmarking," *Archives of Computational Methods in Engineering*, Vol. 10, 2003, pp. 215–296. doi:10.1007/BF02736224
[28] Carrera, E., and Demasi, L., "Classical and Advanced Multilayered Plate Elements Based Upon PVD and RMVT, Part 1: Derivation of Finite Element Matrices," *International Journal for Numerical Methods in Engineering*, Vol. 55, 2002, pp. 191–231. doi:10.1002/nme.492
[29] Carrera, E., and Demasi, L., "Classical and Advanced Multilayered Plate Elements Based Upon PVD and RMVT, Part 2: Numerical Implementations," *International Journal for Numerical Methods in Engineering*, Vol. 55, 2002, pp. 253–291. doi:10.1002/nme.493
[30] Carrera, E., and Giunta, G., "Hierarchical Evaluation of Failure Parameters in Composite Plates," *AIAA Journal*, Vol. 47, 2009, pp. 692–702. doi:10.2514/1.38585
[31] Carrera, E., "Single- vs Multilayer Plate Modelings on the Basis of Reissner's Mixed Theorem," *AIAA Journal*, Vol. 38, 2000, pp. 342–352. doi:10.2514/2.962
[32] Carrera, E., "An Assessment of Mixed and Classical Theories on Global and Local Response of Multilayered Orthotropic Plates," *Composite Structures*, Vol. 50, 2000, pp. 183–198. doi:10.1016/S0263-8223(00)00099-4
[33] Carrera, E., "A Study of Transverse Normal Stress Effect on Vibration of Multilayered Plates and Shells," *Journal of Sound and Vibration*, Vol. 225, 1999, pp. 803–829. doi:10.1006/jsvi.1999.2271
[34] Carrera, E., "Multilayered Shell Theories Accounting for Layerwise Mixed Description, Part 1: Governing Equations," *AIAA Journal*, Vol. 37, 1999, pp. 1107–1116. doi:10.2514/2.821
[35] Carrera, E., "Multilayered Shell Theories Accounting for Layerwise Mixed Description, Part 2: Numerical Evaluations," *AIAA Journal*, Vol. 37, 1999, pp. 1117–1124. doi:10.2514/2.822
[36] Carrera, E., " C_z^0-Requirements—Models for the Two Dimensional Analysis of Multilayered Structures," *Composite Structures*, Vol. 37, 1997, pp. 373–383. doi:10.1016/S0263-8223(98)80005-6
[37] Reissner, E., "On a Certain Mixed Variational Theorem and a Proposed Application," *International Journal for Numerical Methods in Engineering*, Vol. 20, 1984, pp. 1366–1368. doi:10.1002/nme.1620200714
[38] Carrera, E., "Developments, Ideas and Evaluations Based Upon Reissner's Mixed Variational Theorem in the Modeling of Multilayered Plates and Shells," *Applied Mechanics Reviews*, Vol. 54, 2001, pp. 301–329. doi:10.1115/1.1385512
[39] Murakami, H., "Laminated Composite Plate Theory with Improved In-Plane Response," *Journal of Applied Mechanics*, Vol. 53, 1986, pp. 661–666. doi:10.1115/1.3171828
[40] Carrera, E., "On the Use of Murakami's Zig-Zag Function in the Modeling of Layered Plates and Shells," *Computers and Structures*, Vol. 82, 2004, pp. 541–554. doi:10.1016/j.compstruc.2004.02.006
[41] Demasi, L., "Refined Multilayered Plate Elements Based on Murakami Zig-Zag Functions," *Composite Structures*, Vol. 70, 2005, pp. 308–316. doi:10.1016/j.compstruct.2004.08.036
[42] Reddy, J. N., *Mechanics of Laminated Composite Plates and Shells: Theory and Analysis*, 2nd ed., CRC Press, Boca Raton, FL, 2004.
[43] Washizu, K., *Variational Methods in Elasticity and Plasticity*, 2nd ed., Pergamon, New York, 1975.
[44] Palazotto, A. N., and Dennis, S. T., *Nonlinear Analysis of Shell Structures*, AIAA Education Series, AIAA, Washington, D.C., 1992.
[45] Srinivas, S., and Rao, A. K., "Bending, Vibration and Buckling of Simply Supported Thick Orthotropic Rectangular Plates and Laminates," *International Journal of Solids and Structures*, Vol. 6, 1970, pp. 1463–1481. doi:10.1016/0020-7683(70)90076-4
[46] Ye, J. Q., and Soldatos, K. P., "Three-Dimensional Buckling Analysis of Laminated Composite Hollow Cylinders and Cylindrical Panels," *International Journal of Solids and Structures*, Vol. 32, 1995, pp. 1949–1962. doi:10.1016/0020-7683(94)00217-K
[47] Noor, A. K., "Stability of Multilayered Composite Plates," *Fibre Science and Technology*, Vol. 8, 1975, pp. 81–89. doi:10.1016/0015-0568(75)90005-6
[48] Pagano, N. J., "Exact Solutions for Rectangular Bidirectional Composites and Sandwich Plates," *Journal of Composite Materials*, Vol. 4, 1970, pp. 20–34.
[49] Carrera, E., and Brischetto, S., "Analysis of Thickness Locking in Classical, Refined and Mixed Theories for Layered Shells," *Composite Structures*, Vol. 85, 2008, pp. 83–90. doi:10.1016/j.compstruct.2007.10.009
[50] Wu, C. P., and Chen, W. Y., "Vibration and Stability of Laminated Plates Based on a Local High Order Plate Theory," *Journal of Sound and Vibration*, Vol. 177, 1994, pp. 503–520. doi:10.1006/jsvi.1994.1448
[51] Putcha, N. S., and Reddy, J. N., "Stability and Natural Vibration Analysis of Laminated Plates by Using a Mixed Element Based on a Refined Plate Theory," *Journal of Sound and Vibration*, Vol. 104, 1986, pp. 285–300. doi:10.1016/0022-460X(86)90269-5
[52] Di Sciuva, M., and Carrera, E., "Static Buckling of Moderately Thick, Anisotropic, Laminated and Sandwich Cylindrical Shell Panels," *AIAA Journal*, Vol. 28, 1990, pp. 1782–1793. doi:10.2514/3.10474
[53] Noor, A. K., and Peters, J. M., "Stress, Vibration and Buckling of Multilayered Cylinders," *Journal of Structural Engineering*, Vol. 115, 1989, pp. 69–88. doi:10.1061/(ASCE)0733-9445(1989)115:1(69)
[54] Takano, A., "Improvement of Flügge's Equations for Buckling of Moderately Thick Anisotropic Cylindrical Shells," *AIAA Journal*, Vol. 46, 2008, pp. 903–911. doi:10.2514/1.31277
[55] Weaver, P. M., "Design of Laminated Composite Cylindrical Shells Under Axial Compression," *Composites, Part B*, Vol. 31, 2000, pp. 669–679. doi:10.1016/S1359-8368(00)00029-9

F. Pai
Associate Editor